Monthly Notices
of the
ROYAL ASTRONOMICAL SOCIETY

MNRAS **459,** 863–870 (2016)
Advance Access publication 2016 March 18

doi:10.1093/mnras/stw658

Prospects for clustering and lensing measurements with forthcoming intensity mapping and optical surveys

A. Pourtsidou,[1]★ D. Bacon,[1] R. Crittenden[1] and R. B. Metcalf[2]

[1]*Institute of Cosmology and Gravitation, University of Portsmouth, Burnaby Road, Portsmouth PO1 3FX, UK*
[2]*Dipartimento di Fisica e Astronomia, Alma Mater Studiorum Universitá di Bologna, viale Berti Pichat, 6/2, I-40127 Bologna, Italy*

Accepted 2016 March 16. Received 2016 March 16; in original form 2015 September 29

ABSTRACT

We explore the potential of using intensity mapping surveys (MeerKAT, SKA) and optical galaxy surveys (DES, LSST) to detect H I clustering and weak gravitational lensing of 21 cm emission in auto- and cross-correlation. Our forecasts show that high-precision measurements of the clustering and lensing signals can be made in the near future using the intensity mapping technique. Such studies can be used to test the intensity mapping method, and constrain parameters such as the H I density $\Omega_{\rm H\,I}$, the H I bias $b_{\rm H\,I}$ and the galaxy-H I correlation coefficient $r_{\rm H\,I-g}$.

Key words: gravitational lensing: weak – cosmology: observations – cosmology: theory – large-scale structure of Universe.

1 INTRODUCTION

Intensity mapping (Battye, Davies & Weller 2004; Chang et al. 2008; Loeb & Wyithe 2008; Mao et al. 2008; Peterson et al. 2009; Seo et al. 2010; Ansari et al. 2012; Battye et al. 2013; Switzer et al. 2013; Bull et al. 2015) is an innovative technique that uses neutral hydrogen (H I) to map the large-scale structure (LSS) of the Universe in three dimensions. Instead of detecting individual galaxies like the conventional galaxy surveys, intensity mapping surveys use H I as a dark matter tracer by measuring the intensity of the redshifted 21 cm line across the sky and along redshift, treating the 21 cm sky as a diffuse background, similar to the Cosmic Microwave Background (CMB).

Santos et al. (2015) investigated the potential of the planned Square Kilometre Array[1] (SKA) to deliver H I intensity mapping maps over a broad range of frequencies and a substantial fraction of the sky. Detecting the 21 cm signal in auto- and cross-correlation using intensity mapping and optical galaxy surveys is essential in order to exploit the intensity mapping technique, test foreground removal methods, and identify and control systematic effects. This is possible using SKA pathfinders like MeerKAT[2] and, as we will show, in many cases high signal-to-noise ratio (S/N) measurements can be achieved.

Cross-correlation between LSS traced by galaxies and 21 cm intensity maps at $z \sim 1$ was first detected using the Green Bank Telescope (GBT) and the DEEP2 optical galaxy redshift survey (Chang et al. 2010); this measurement was improved using the GBT and the WiggleZ Dark Energy Survey (Masui et al. 2013). The auto-power spectrum of 21 cm intensity fluctuations using data acquired with the GBT was used in Switzer et al. (2013) to constrain H I fluctuations at $z \sim 0.8$ and was interpreted as an upper bound on the 21 cm signal because of residual foreground contamination bias.

In this work we present H I detection forecasts for auto- and cross-correlation measurements using intensity mapping surveys with MeerKAT and SKA, and optical galaxy surveys with the Dark Energy Survey (DES)[3] and the Large Synoptic Survey Telescope (LSST)[4]. Our forecasts concern both the H I intensity fluctuations as well as the weak gravitational lensing of 21 cm emission, using the weak lensing intensity mapping method developed in Pourtsidou & Metcalf (2014, 2015). In the following we denote the density fluctuations δ using the subscript H I for 21 cm and g for galaxies. We also denote the lensing convergence κ using the subscript g when it is detected using galaxies and IM when using the intensity mapping method.

In Section 2 we introduce the H I intensity mapping and optical galaxy surveys we are going to use for our clustering and lensing measurements forecasts and analyse their noise properties. In Section 3 we study correlations of the H I observables. We investigate the possibility of measuring the H I–H I power spectrum ($\delta_{\rm H\,I} \times \delta_{\rm H\,I}$) with MeerKAT and show forecasts for the lensing convergence power spectrum measurements ($\kappa_{\rm IM} \times \kappa_{\rm IM}$) and for $\delta_{\rm H\,I} \times \kappa_{\rm IM}$ using MeerKAT/SKA Phase 1 (SKA1) and the intensity mapping method. Cross-correlation studies are less susceptible to systematic contamination than auto-correlations, and can be observed when the noise

★ E-mail: alkistis.pourtsidou@port.ac.uk
[1] www.skatelescope.org
[2] http://www.ska.ac.za/meerkat/
[3] http://www.darkenergysurvey.org/
[4] http://www.lsst.org/

levels in the H I observations are relatively high. We study these in Section 4. First we examine the possibility of measuring the $\delta_{\rm H\,I} \times \delta_g$ and $\delta_{\rm H\,I} \times \kappa_g$ correlations using MeerKAT and DES. We then study the $\delta_g \times \kappa_{\rm IM}$ correlation with LSST and MeerKAT/SKA1. Finally, we investigate $\kappa_g \times \kappa_{\rm IM}$ with LSST and SKA1.

There are exciting prospects for performing clustering and lensing measurements with the forthcoming intensity mapping and optical surveys. The S/N for many of the cross and auto-spectra we consider is high, so significant progress will occur in the near future, exploiting SKA pathfinders and near-term optical galaxy surveys. The primary goal of our work is to show that it is possible to perform high-precision clustering and lensing studies in three dimensions using the intensity mapping technique. We can use these measurements to calibrate the neutral gas density $\Omega_{\rm H\,I}$, the H I bias parameter $b_{\rm H\,I}$ and the galaxy-H I correlation coefficient $r_{\rm H\,I-g}$. The current uncertainties in the H I density fraction $\Omega_{\rm H\,I}$ and the bias $b_{\rm H\,I}$ are large; for example, the best constraint obtained so far for the H I density–H I bias combination is $\Omega_{\rm H\,I} b_{\rm H\,I} = 4.3 \pm 1.1 \times 10^{-4}$ at $z \sim 0.8$ (Switzer et al. 2013). Their precise values and evolution across redshift are very important for the S/N of the clustering and lensing measurements, as they determine the amplitude of the H I signal. As shown in Bull et al. (2015), $\Omega_{\rm H\,I}(z)$ substantially affects the forecasted cosmological constraints using late-time intensity mapping clustering surveys, and it is also very important for the 21cm lensing S/N from post-reionization source redshifts (Pourtsidou & Metcalf 2015). Therefore, it is crucial to utilize near term intensity mapping surveys in order to tightly constrain them. Forecasted constraints on the H I parameters and other cosmological parameters using clustering and lensing measurements will be the subject of future work.

2 THE SURVEYS

2.1 H I INTENSITY MAPPING

We consider a range of H I surveys, focusing on the SKA and its pathfinder MeerKAT. There are two different observing modes we can consider, namely the single-dish mode and the interferometer mode (see Bull et al. 2015 for details). Below we describe the noise properties for both modes.

2.1.1 Single-dish mode

The SKA-MID instrument is primarily an interferometer, but there are also discussions and plans to operate it in single-dish mode as well, in order to collect total power (auto-correlation) data (Santos et al. 2014, 2015; Bull et al. 2015). This is crucial for cosmological measurements with the SKA and the H I intensity mapping technique. For example, arrays with large dishes do not adequately sample BAO scales at low redshifts in interferometer mode, as the largest scale probed is limited by the dish size. Using the single-dish mode and covering a large fraction of the sky ultra large scales can be measured and the constraints obtained are competitive with state-of-the-art optical galaxy surveys like Euclid (Amendola et al. 2013; Santos et al. 2015).

MeerKAT is a 64-dish SKA pathfinder on the planned site of SKA1-MID and it will start observing in 2016 with at least 16 dishes. From here onwards, we will refer to its first phase as MeerKAT-16, and its full phase as MeerKAT. The dishes have 13.5 m diameter with number of beams $N_{\rm beams} = 1$; the redshift (frequency) range is $0 < z < 1.45$ ($580 < f < 1420$ MHz) for the 21 cm line and the frequency resolution $\Delta f = 50$ kHz. The system temperature is taken to be $T_{\rm sys} = 25$ K. The sky area and total observing time are determined by the survey strategy. We will consider two strategies: First, we assume a sky area $A_{\rm sky} = 1000\,{\rm deg}^2$ and a total observation time of 3 weeks, and then we repeat the calculation with $A_{\rm sky} = 5000\,{\rm deg}^2$ and a total observation time of 15 weeks.

The noise properties of such measurements have been described in various works (see, for example, Battye et al. (2013)) and depend on the instrumental noise in a given pixel (beam), its volume, and the instrumental response, modelled by the window function $W(k)$. Because the frequency resolution in such surveys is very good (of the order of tens of kHz) we can ignore the instrument response function in the radial direction. However, there is a window function related to the finite angular resolution:

$$W^2(k) = \exp\left[-k^2\chi(z)^2\left(\frac{\theta_{\rm B}}{\sqrt{8\ln 2}}\right)^2\right], \tag{1}$$

where $\chi(z)$ is the comoving radial distance at redshift z and $\theta_{\rm B} \sim \lambda/D_{\rm dish}$ the beam FWHM of a single dish with diameter $D_{\rm dish}$ at wavelength λ. Considering a redshift bin with limits $z_{\rm min}$ and $z_{\rm max}$, the survey volume will be given by

$$V_{\rm sur} = \Omega_{\rm tot}\int_{z_{\rm min}}^{z_{\rm max}} {\rm d}z \frac{{\rm d}V}{{\rm d}z{\rm d}\Omega} = \Omega_{\rm tot}\int_{z_{\rm min}}^{z_{\rm max}} {\rm d}z \frac{c\chi(z)^2}{H(z)}, \tag{2}$$

and $\Omega_{\rm tot} = A_{\rm sky}$, the sky area the survey scans. The pixel's volume $V_{\rm pix}$ is also calculated from equation (2), but with

$$\Omega_{\rm pix} \simeq 1.13\theta_B^2 \tag{3}$$

assuming a Gaussian beam, and the corresponding pixel z-limits corresponding to the channel width Δf. Finally, the pixel noise $\sigma_{\rm pix}$ is given by

$$\sigma_{\rm pix} = \frac{T_{\rm sys}}{\sqrt{\Delta f\, t_{\rm total}(\Omega_{\rm pix}/\Omega_{\rm tot})N_{\rm dishes}N_{\rm beams}}}, \tag{4}$$

with $N_{\rm dishes}$ the number of dishes.

Here we should note that various systematic effects might lead to an increase of the actual noise in the autocorrelation measurements. For example, in addition to the thermal noise quantified above these observations suffer from correlated $(1/f)$ noise and ground pickup. However, recent work on the subject suggests that these effects can be removed to a large extent (Bigot-Sazy et al. 2015). Other systematics include real beams with sidelobes and mis-calibration which will lead to mode-mixing and thus affect the foreground subtraction.

The MeerKAT radio telescope is a precursor to the SKA telescope and will be integrated into the mid-frequency component of SKA1 (SKA1-MID). As we will see below, MeerKAT can also be used as an interferometer in its own right.

2.1.2 Interferometer mode

The thermal noise power spectrum for an interferometer array is given by (White et al. 1999; Zaldarriaga, Furlanetto & Hernquist 2004)

$$C_\ell^{\rm N} = \frac{(2\pi)^2 T_{\rm sys}^2}{B t_u d^2\ell}, \tag{5}$$

where B is the total bandwidth of the observation, t_u is the time each visibility is observed, and ℓ is related to the Fourier wavenumber u by $\ell = 2\pi u$ – consequently, the Fourier space pixel $d^2\ell$ is related to

the square resolution element d^2u by $d^2\ell = (2\pi)^2 d^2u$. The observation time per visibility t_u is given by (Zaldarriaga et al. 2004; Mao et al. 2008)

$$t_u = \frac{A_{\rm dish}}{\lambda^2} t_0 n(u), \tag{6}$$

where $A_{\rm dish}$ is the area of an individual dish, t_0 is the total observation time and $n(u)$ – or, equivalently, $n(\ell)$ – is the number density of baselines.

Using the above we finally get

$$C_\ell^{\rm N} = \frac{T_{\rm sys}^2 [{\rm FOV}]^2}{B t_0 n(\ell)}. \tag{7}$$

Here we have used the fact that the primary beam size (and hence d^2u) is related to the area of the dishes, so we can use the approximation $A_{\rm dish} = \lambda^2 d^2u$ (Zaldarriaga et al. 2004), and $1/{\rm FOV} \equiv A_{\rm dish}/\lambda^2$ (where FOV is the field of view, and λ is the observing wavelength). The required $n(\ell)$ distributions to calculate the noise of SKA1-MID and MeerKAT in interferometer mode are taken from Bull et al. (2015). The system temperature $T_{\rm sys}$ is the sum of the sky and receiver noise and is approximately given by (the $T_{\rm sys}$ values are nominal and depend on the sky and the receivers) (Dewdney 2013)

$$T_{\rm sys} = 28 + 66 \left(\frac{\nu}{300\,{\rm MHz}} \right)^{-2.55} {\rm K}, \tag{8}$$

with ν the observing frequency. We also note that using the uniform approximation formula for the number density of baselines in equation (7), $n(\ell) \simeq (2\pi) N_{\rm dishes}^2 / \ell_{\rm max}^2$, we recover the widely known uniform $C_\ell^{\rm N}$ formula (see, for example, Zaldarriaga et al. 2004).

The thermal noise of the interferometer is part of the lensing reconstruction noise using the lensing estimator developed in Pourtsidou & Metcalf (2015). In that work the method of 21 cm intensity mapping was used to study gravitational lensing over a wide range of post-reionization redshifts – this extends weak lensing measurements to higher redshifts than are accessible with conventional galaxy surveys. Detecting κ with this method would be an important science achievement of the intensity mapping technique.

Central to this detection is understanding $N_\kappa(\ell)$, the lensing reconstruction noise using the aforementioned method. The expression for $N_\kappa(\ell)$ is rather lengthy, so we will not include it here, but the interested reader is referred to Pourtsidou & Metcalf (2015), Appendix C. To summarize, the lensing reconstruction noise involves the underlying dark matter power spectrum $P_{\delta\delta}$, the H I density $\Omega_{\rm H\,I}(z)$ as well as the H I mass (or luminosity) moments up to fourth order and, as already stated, the thermal noise of the instrument $C_\ell^{\rm N}$. Note that in the following we will assume an observation (H I source) redshift $z_s = 1.4$ corresponding to a frequency of 592 MHz, bandwidth $B = 40$ MHz corresponding to $\Delta z \sim 0.15$, total observation time $t_0 = 4000$ h and sky area $A_{\rm sky} = 25\,000\,{\rm deg}^2$ when we consider MeerKAT and SKA1 in interferometer mode. We remind the reader that the frequency (redshift) range for MeerKAT is $580 < z < 1420$ MHz ($0 < z < 1.45$), while for SKA1-MID $350 < f < 1050$ MHz ($0.35 < z < 3.06$) (Band 1) (Bull et al. 2015).

2.2 Optical galaxy surveys

We consider two photometric surveys: the ongoing Dark Energy Survey (DES) and the planned Large Synoptic Survey Telescope (LSST). DES aims to investigate the nature of the cosmic acceleration and combines four probes of Dark Energy, namely Type Ia Supernovae, Baryonic Acoustic Oscillations (BAOs), galaxy clusters and weak gravitational lensing. LSST is a ground-based, wide field survey telescope. One of its main goals is to provide multiple probes of dark energy, with the two most powerful being weak gravitational lens tomography and BAOs.

The DES survey parameters are (Becker et al. 2015) $A_{\rm sky} = 5000\,{\rm deg}^2$, number density of galaxies $n_g = 10\,{\rm arcmin}^{-2}$, redshift range $0 < z < 2$ with median redshift $z_0 = 0.7$. The LSST survey parameters are assumed to be $f_{\rm sky} = 0.5$, number density of galaxies $n_g = 40\,{\rm arcmin}^{-2}$, redshift range $0 < z < 2$ with median redshift $z_0 = 1$ (Abell et al. 2009). The redshift distribution for galaxy surveys like DES and LSST (and Euclid) has the form (Abell et al. 2009; Amendola et al. 2013; Becker et al. 2015)

$$\frac{{\rm d}n}{{\rm d}z} \propto z^\alpha \exp[-(z/z_0)^\eta]. \tag{9}$$

For our forecasts we will use the common parametrization $\alpha = 2$, $\eta = 3/2$.

For these surveys, the primary noise for density measurements arises from shot noise, with the shot noise contribution given by

$$P^{\rm shot} = \frac{1}{(N_g/V_{\rm sur})}, \tag{10}$$

with N_g the number of galaxies within the redshift bin under consideration.

These optical surveys can constrain weak lensing via shear measurements. The noise associated with the estimated weak lensing convergence is given by $\sigma_\kappa^2/\bar{n}_b$, where σ_κ is the shape noise of each background galaxy and $\bar{n}_b$ is the number density of background galaxies in the chosen source bin. In the following we assume $\sigma_\kappa = 0.3$ (Schmidt et al. 2012).

3 H I ALONE

In this section we investigate auto-correlations of the H I observables, and we show that high signal-to-noise H I detection can be achieved with near-future facilities like MeerKAT-16, hence there are very good prospects for testing and using the intensity mapping method very soon. Lensing of 21 cm sources using the intensity mapping method requires more powerful instruments like the SKA, and heavily depends on the H I density evolution with cosmic time.

3.1 $\delta_{\rm H\,I} \times \delta_{\rm H\,I}$ with MeerKAT-16

The detection of H I in autocorrelation using the intensity mapping method is the primary science goal of an intensity mapping instrument. The power spectrum of the H I fluctuations, $\delta_{\rm H\,I}$, is assumed to take the form

$$P_{\rm H\,I}(k, z) = \bar{T}(z)^2 b_{\rm H\,I}(z)^2 P_{\delta\delta}(k, z), \tag{11}$$

where $P_{\delta\delta}$ is the underlying dark matter density power spectrum and $b_{\rm H\,I}$ the H I bias. The mean H I brightness temperature at redshift z is given by (Battye et al. 2013)

$$\bar{T}(z) = 180\,\Omega_{\rm H\,I}(z) h \frac{(1+z)^2}{H(z)/H_0}\,{\rm mK}. \tag{12}$$

For our forecasts here and in the next sections we will use $b_{\rm H\,I}(z)$ from Camera et al. (2013) and assume

$$\Omega_{\rm H\,I}(z) = 4 \times 10^{-4} (1+z)^{0.6} \tag{13}$$

which has been suggested in Crighton et al. (2015). We also use the fitting formula by Smith et al. (2003) for the non-linear power spectrum.

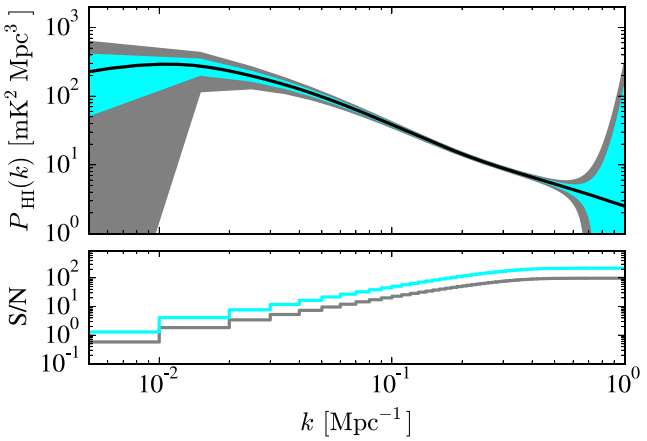

Figure 1. H I detection in autocorrelation with MeerKAT-16. The upper panel shows the predicted power spectrum $P_{\rm H\,I}(k, z_c)$ at $z_c = 0.1$ (black solid line). The grey area represents the measurement errors $\delta P_{\rm H\,I}$ taking $A_{\rm sky} = 1000\,{\rm deg}^2$ and a total observation time of 3 weeks, while the cyan area corresponds to $A_{\rm sky} = 5000\,{\rm deg}^2$ and a total observation time of 15 weeks. The lower panel shows the cumulative S/N defined in equation (15).

The uncertainty on a power spectrum measurement averaged over a radial bin in k-space of width Δk is (Battye et al. 2013)

$$\delta P_{\rm H\,I} = \sqrt{2\frac{(2\pi)^3}{V_{\rm sur}}\frac{1}{4\pi k^2 \Delta k}}\left[P_{\rm H\,I} + \sigma_{\rm pix}^2 V_{\rm pix} W^{-2}\right], \quad (14)$$

where the pixel noise, pixel volume and response window function were described in the previous Section.

The results for H I detection in autocorrelation at a central redshift $z_c = 0.1$ with a redshift bin width $\Delta z = 0.2$ using MeerKAT-16 and the two aforementioned survey strategies (three weeks and $A_{\rm sky} = 1000\,{\rm deg}^2$, 15 weeks and $A_{\rm sky} = 5000\,{\rm deg}^2$) are shown in Fig. 1, using $\Delta k = 0.01\,{\rm Mpc}^{-1}$. We plot the cumulative S/N, defined as

$$\frac{\rm S}{\rm N} = \sqrt{\sum_k \left(\frac{P_{\rm H\,I}}{\delta P_{\rm H\,I}}\right)^2}. \quad (15)$$

As can be seen, these measurements are very precise across a wide range of scales and we can use them to calibrate the combination $\Omega_{\rm H\,I} b_{\rm H\,I}$. Note that since MeerKAT will cover a wide redshift range $0 < z < 1.45$, we can use tomography to probe the combination $\Omega_{\rm H\,I} b_{\rm H\,I}$ at different redshifts.

3.2 $\kappa_{\rm IM} \times \kappa_{\rm IM}$ with MeerKAT/SKA1

The lensing convergence power spectrum from sources at redshift z_s is given by the expression (Kaiser 1992, 1998)

$$C_{\kappa\kappa}(\ell) = \frac{9\Omega_m^2 H_0^3}{4c^3}\int_0^{z_s} {\rm d}z \frac{P_{\delta\delta}(k = \ell/\chi, z)}{a^2 H(z)/H_0}\left[\frac{\hat{\chi}_s - \chi}{\hat{\chi}_s}\right]^2, \quad (16)$$

with $\hat{\chi}_s \equiv \chi(z_s)$. The uncertainty in the measurement of the power spectrum is

$$\delta C_{\kappa\kappa}(\ell) = \sqrt{\frac{2}{(2\ell+1)\Delta\ell\, f_{\rm sky}}}\left(C_{\kappa\kappa}(\ell) + N_\kappa(\ell)\right), \quad (17)$$

where $N_\kappa(\ell)$ is the lensing reconstruction noise using the intensity mapping method described in the previous section.

In Pourtsidou & Metcalf (2015) it was found that the S/N is strongly dependent on the possible evolution of the H I mass function. More specifically, it was shown that assuming the no-evolution scenario (which is the most conservative, but also less realistic approach), precise measurements can only be made with an SKA2-like instrument; however assuming instead a model where the H I density $\Omega_{\rm H\,I}(z)$ increases by a factor of 5 by redshift $z = 3$ and then slowly decreases towards redshift $z = 5$, as suggested by the DLA observations from Peroux et al. (2003) (for more recent results in the redshift range $2 < z < 5$ see Sánchez-Ramírez et al. (2016)), high S/N can be achieved even with SKA1.

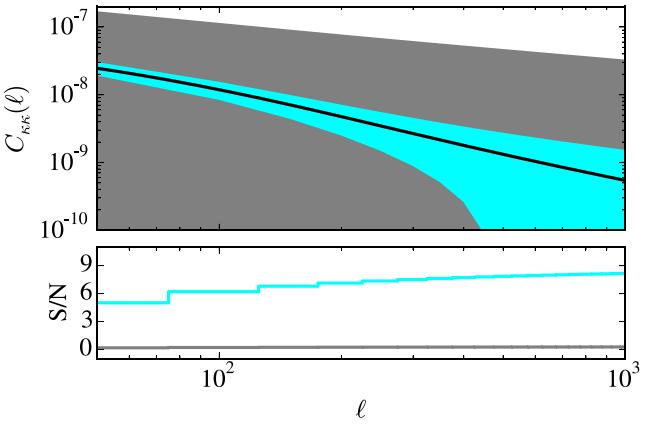

Figure 2. The upper panel shows the convergence power spectrum and measurement errors with MeerKAT (grey) and SKA1 (cyan), using the intensity mapping method. The lower panel shows the cumulative S/N ratio. Sources are at $z_s = 1.4$.

In this work we instead use the H I evolution model given by equation (13), which fits observations in a wide redshift range, and we implement this evolution in the $\phi^\star$ parameter of the H I mass function which is locally measured by the HIPASS survey (Zwaan et al. 2003). We also note that in Pourtsidou & Metcalf (2015) the telescope distribution within the array was approximated as uniform for the calculation of the thermal noise component, while here we use the baseline designs from Bull et al. (2015). In Fig. 2 we show results for MeerKAT and SKA1 assuming H I sources are at $z_s = 1.4$ and using $\Delta\ell = 50$.

As we can see, we can detect lensing using the intensity mapping method and SKA1, but using MeerKAT detection in autocorrelation is not possible. However, below we will demonstrate that cross-correlations can enhance the S/N of the lensing measurements.

3.3 $\delta_{\rm H\,I} \times \kappa_{\rm IM}$ with MeerKAT/SKA1

We are going to examine the correlation of a foreground (f) density tracer field with the background (b) convergence κ field, where both are probed by the IM survey.

Using the Limber approximation (Limber 1954) the angular cross-power spectrum $C_{{\rm H\,I}\kappa}$ is given by

$$C_{{\rm H\,I}\kappa}(\ell) = \frac{3\Omega_{\rm m} H_0^2}{2c^2}\int \frac{{\rm d}\chi_f}{a(\chi_f)} W_f(\chi_f)\int {\rm d}\chi_b W_b(\chi_b) \times \frac{\chi_b - \chi_f}{\chi_b \chi_f}$$
$$\bar{T}(\chi_f) r_{\rm H\,I} b_{\rm H\,I}(\chi_f) P_{\delta\delta}\left(\frac{\ell}{\chi_f}, \chi_f\right), \quad (18)$$

where χ is the comoving distance, W_f (W_b) the foreground (background) redshift distribution and $r_{\rm H\,I}$ is a correlation coefficient quantifying the potential stochasticity between the dark matter density and the H I density fields. If the foreground lens slice is narrow enough in redshift ($\Delta z \sim 0.1$ is sufficient), we can approximate the

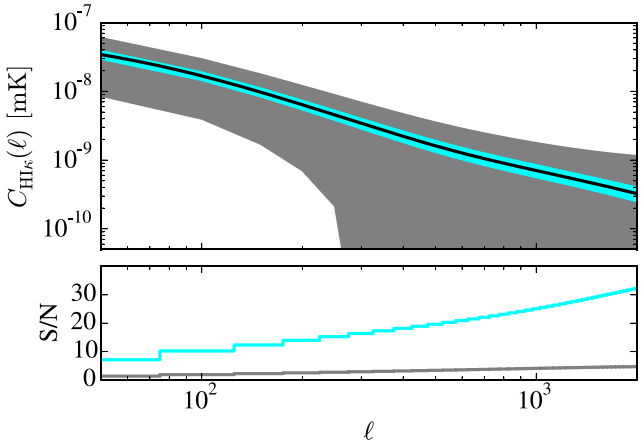

Figure 3. The upper panel shows the $C_{\mathrm{H}\,\textsc{i}\kappa}$ cross-correlation power spectrum and measurement errors with MeerKAT (grey) and SKA1 (cyan). The lower panel shows the cumulative S/N ratio.

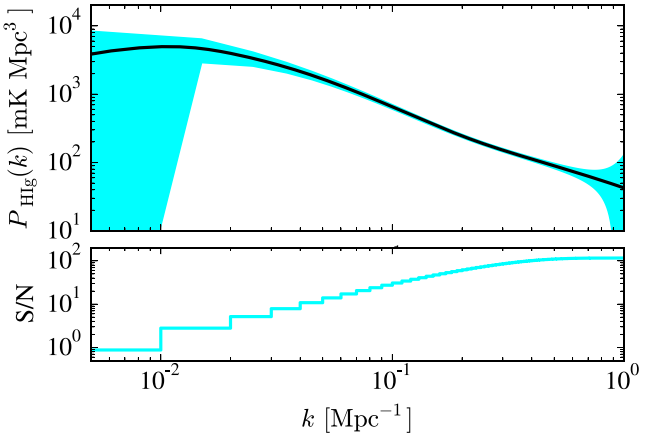

Figure 4. The upper panel shows the $P_{\mathrm{H}\,\textsc{i},\mathrm{g}}$ cross-correlation power spectrum and measurement errors with MeerKAT-16 and DES. The lower panel shows the cumulative S/N. Note $t_{\mathrm{total}} = 1$ week for MeerKAT-16.

foreground redshift distribution as a delta function at a distance $\hat{\chi}_f$, $W_f(\chi_f) = \delta^{\mathrm{D}}(\chi_f - \hat{\chi}_f)$. We also use the delta function approximation at a distance $\hat{\chi}_b$ for the distribution of the 21 cm sources. We then find

$$C_{\mathrm{H}\,\textsc{i}\kappa}(\ell) = \frac{3\Omega_{\mathrm{m}}H_0^2}{2c^2}\left(\frac{\bar{T}(\hat{\chi}_f)r_{\mathrm{H}\,\textsc{i}}b_{\mathrm{H}\,\textsc{i}}(\hat{\chi}_f)P_{\delta\delta}\left(\frac{\ell}{\hat{\chi}_f},\hat{\chi}_f\right)}{a(\hat{\chi}_f)\hat{\chi}_f}\right)\frac{\chi_b-\hat{\chi}_f}{\chi_b}.$$

It is useful to translate the H I power into multipole space,

$$C_{\mathrm{H}\,\textsc{i}-\mathrm{H}\,\textsc{i}}(\ell) = \int \mathrm{d}z E(z)W^2(z)[\bar{T}(z)]^2 P_{\delta\delta}(\ell/\chi(z),z)/\chi^2(z), \quad (19)$$

with $W(z)$ a projection kernel which we take to be a top-hat function equal to $1/\Delta z$ within the redshift bin and 0 otherwise.

The uncertainty in the cross-correlation, for a bin of width $\Delta\ell$ and for a survey scanning a fraction of the sky f_{sky}, is

$$\delta C_{\mathrm{H}\,\textsc{i}\kappa}(\ell) = \sqrt{\frac{2}{(2\ell+1)\Delta\ell f_{\mathrm{sky}}}} \times \sqrt{C^2_{\mathrm{H}\,\textsc{i}\kappa}(\ell) + (C_{\mathrm{H}\,\textsc{i}-\mathrm{H}\,\textsc{i}}(\ell)+N(\ell))(C_{\kappa\kappa}(\ell)+N_\kappa(\ell))}, \quad (20)$$

with $N_\kappa(\ell)$ from Pourtsidou & Metcalf (2014, 2015). For the single-dish mode, the noise term $N(\ell)$ is given by (Battye et al. 2013)

$$N(\ell) = \Omega_{\mathrm{pix}}(\sigma_{\mathrm{pix}})^2 \exp\left[\ell(\ell+1)(\theta_B/\sqrt{8\ln 2})^2\right], \quad (21)$$

with $\sigma_{\mathrm{pix}} = T_{\mathrm{sys}}/\sqrt{2\Delta f t_{\mathrm{obs}}}$ (the $1/\sqrt{2}$ factor comes from assuming dual polarization). For the interferometer mode, $N(\ell) = C_\ell^{\mathrm{N}}$, defined in equation (7).

The results are shown in Fig. 3 assuming the MeerKAT and SKA1 parameters in interferometer mode. The foreground central redshift is $z_c = 0.5$ with $\Delta z = 0.1$. We see that using MeerKAT in interferometer mode we have the possibility of detecting the lensing convergence in cross-correlation with the H I density using the intensity mapping method (with a cumulative S/N ~ 5). With SKA1 we can achieve a high S/N detection. Using tomography (for example, taking different foreground bins z_c) we can perform measurements with a similar S/N level along the redshift (frequency) direction.

4 CROSS-CORRELATING WITH GALAXY SURVEYS

As we saw above, the prospects for detecting the H I density fluctuations are very good even for a near-term instrument such as MeerKAT-16; however, the measurement of convergence with H I intensity mapping might require an advanced SKA measurement. We also showed that cross-correlating the density and convergence using an IM survey can greatly improve the S/N for the lensing detection. It is interesting to examine to what extent the H I detections could be accelerated by cross-correlating these measurements with density and convergence derived from galaxy surveys, where the noise and potential systematics are expected to be independent.

For the purposes of these projections we assume that the galaxy power spectrum is related to the density by $P_{gg}(k,z) = b_g^2 P_{\delta\delta}(k,z)$ and assume the galaxy bias $b_g(z)$ evolves as $\sqrt{1+z}$ (Rassat et al. 2008). In addition, there is potential stochasticity between the dark matter density and the galaxy density fields; this is quantified by the correlation coefficient r_g.

4.1 $\delta_{\mathrm{H}\,\textsc{i}} \times \delta_g$ with MeerKAT-16 and DES

The $\delta_{\mathrm{H}\,\textsc{i}} \times \delta_g$ combination, i.e. the cross-correlation between a 21 cm intensity map with LSS traced by galaxies has been investigated previously (Chang et al. 2010; Masui et al. 2013) at redshift $z \sim 1$. This correlation constrains $\Omega_{\mathrm{H}\,\textsc{i}}b_{\mathrm{H}\,\textsc{i}}r_{\mathrm{H}\,\textsc{i}-\mathrm{g}}$. For this cross-correlation power spectrum

$$P_{\mathrm{H}\,\textsc{i},\mathrm{g}}(k) = \bar{T}b_{\mathrm{H}\,\textsc{i}}b_g r_{\mathrm{H}\,\textsc{i}-\mathrm{g}}P_{\delta\delta}(k), \quad (22)$$

the uncertainty averaged over a radial bin in k-space of width Δk is

$$\delta P_{\mathrm{H}\,\textsc{i},\mathrm{g}} = \sqrt{2\frac{(2\pi)^3}{V_{\mathrm{sur}}}\frac{1}{4\pi k^2\Delta k}} \times \sqrt{P^2_{\mathrm{H}\,\textsc{i},\mathrm{g}} + \left(P_{\mathrm{H}\,\textsc{i}} + \sigma^2_{\mathrm{pix}}V_{\mathrm{pix}}W^{-2}\right)(P_{gg}+P^{\mathrm{shot}})}, \quad (23)$$

where the H I noise and shot noise terms were defined above. black For our forecasts here we will set $r_{\mathrm{H}\,\textsc{i}-\mathrm{g}} = 1$ for simplicity. We will assume MeerKAT-16 measurements with $A_{\mathrm{sky}} = 5000\,\mathrm{deg}^2$ and a total observing time of 1 week for this case, and combine it with DES. The redshift bin we use is $0 < z < 0.2$ with central redshift $z_c = 0.1$. As we can see from Fig. 4, these measurements are

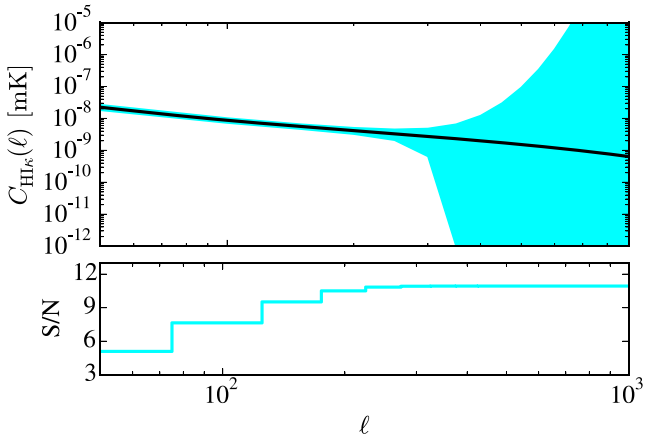

Figure 5. The upper panel shows the $C_{\mathrm{H\,I}\kappa}$ cross-correlation power spectrum and measurement errors with MeerKAT-16 and DES. The lower panel shows the cumulative S/N.

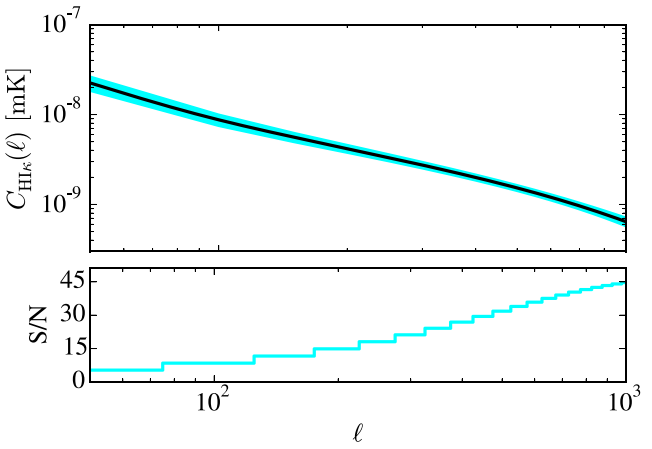

Figure 6. The upper panel shows the $C_{\mathrm{H\,I}\kappa}$ cross-correlation power spectrum and measurement errors with MeerKAT (in interferometer mode) and DES. The lower panel shows the cumulative S/N.

very precise across a wide range of scales even if a single week's observing time is used.

We will also be able to perform tomographic studies across the redshift range $0 < z < 1.45$, constraining the $\Omega_{\mathrm{H\,I}} b_{\mathrm{H\,I}} r_{\mathrm{H\,I-g}}$ combination as a function of redshift. As we discussed in the introduction, constraining $\Omega_{\mathrm{H\,I}}$ is very important for exploiting the power of intensity mapping surveys for cosmology. Performing the aforementioned tomographic studies would measure the late-time evolution of the H I parameters which determine the overall amplitude of the H I signal and, consequently, the S/N of the clustering measurements. In Switzer et al. (2013), for example, the measurement of $\Omega_{\mathrm{H\,I}} b_{\mathrm{H\,I}} r_{\mathrm{H\,I-g}}$ was taken as a lower bound of $\Omega_{\mathrm{H\,I}} b_{\mathrm{H\,I}}$ and then combined with the upper bound coming from H I autocorrelation measurements to a determination of $\Omega_{\mathrm{H\,I}} b_{\mathrm{H\,I}}$ at $z \sim 0.8$. As mentioned in the same paper, redshift space distortions can be utilized in order to break the degeneracy between the H I bias and H I density parameters (Wyithe 2008; Masui, McDonald & Pen 2010).

4.2 $\delta_{\mathrm{H\,I}} \times \kappa_g$ with MeerKAT and DES

We are now going to examine the cross-correlation of the H I density fluctuations with the lensing convergence using a galaxy survey.

The formulae used for the signal and error calculations are the same as in the $\delta_{\mathrm{H\,I}} \times \kappa_{\mathrm{IM}}$ case but instead of the IM lensing reconstruction noise $N_\kappa(\ell)$ we have the galaxy survey shape noise $\sigma_\kappa^2/\bar{n}_b$.

For DES lensing measurements, we consider a source bin with $z_b = 1.5$ and width $\Delta z = 1.0$. The chosen width contains a large number of galaxies, which translates to a low shape noise in the lensing convergence measurement. As already stated, we always assume $\sigma_\kappa = 0.3$ (Schmidt et al. 2012). For MeerKAT we use a bin with central redshift $z_c = 0.1$ and width $\Delta z \simeq 0.08$ (equivalently, $\Delta f = 100\,\mathrm{MHz}$), with $t_{\mathrm{total}} = 15$ weeks. We also take $A_{\mathrm{sky}} = 5000\,\mathrm{deg}^2$ and $\Delta\ell = 50$. The results for MeerKAT-16 are shown in Fig. 5 – note that the dominant noise term is from the H I noise $N(\ell)$ defined in equation (21) which diverges as we reach the limits set by the beam resolution.

In Fig. 6 we show the results for the full MeerKAT, instead in interferometer mode. One can see that this mode allows smaller scales to be probed with significant signal to noise. These measurements can constrain the $\Omega_{\mathrm{H\,I}} b_{\mathrm{H\,I}} r_{\mathrm{H\,I}}$ combination. Using tomography this can be achieved across a wide range of redshift, which is very important as there is currently a lot of uncertainty regarding the H I evolution with cosmic time.

4.3 $\delta_g \times \kappa_{\mathrm{IM}}$ with LSST and MeerKAT/SKA1

A very interesting combination to consider is the cross-correlation of the galaxy density field with the lensing convergence probed via the intensity mapping method. Cross-correlating κ_{IM} with δ_g can help boost the S/N of the κ detection using the method developed in Pourtsidou & Metcalf (2015) and also remove systematic effects since optical and intensity mapping surveys use completely different instruments and strategies. In this case we have

$$C_{g\kappa}(\ell) = \frac{3\Omega_{\mathrm{m}} H_0^2}{2c^2} \left(\frac{r_g b_g(\hat{\chi}_f) P_{\delta\delta}\left(\frac{\ell}{\hat{\chi}_f}, \hat{\chi}_f\right)}{a(\hat{\chi}_f)} \right) \frac{\hat{\chi}_s - \hat{\chi}_f}{\hat{\chi}_f \hat{\chi}_s}. \quad (24)$$

The corresponding uncertainty is

$$\delta C_{g\kappa}(\ell) = \sqrt{\frac{2}{(2\ell+1)\Delta\ell f_{\mathrm{sky}}}} \times \sqrt{C_{g\kappa}^2(\ell) + \left(C_{\mathrm{gg}}(\ell) + \frac{1}{\bar{n}_g}\right)(C_{\kappa\kappa}(\ell) + N_\kappa(\ell))}. \quad (25)$$

Here

$$C_{\mathrm{gg}}(\ell) = \int \mathrm{d}z E(z) W^2(z) P_{\delta\delta}(\ell/\chi(z), z)/\chi^2(z) \quad (26)$$

and $\bar{n}_g$ is the number density of galaxies in the redshift bin under consideration.

We show results in Fig. 7 combining LSST and SKA1, as well as LSST and MeerKAT, with the 21 cm sources at redshift $z_s = 1.4$ and the foreground density tracer field at $z_f = 1.0$ with $\Delta z_f = 0.2$. We use $\Delta\ell = 50$.

We see that a high signal-to-noise detection can be achieved with SKA1 in combination with an optical survey like LSST. Comparing with the H I autocorrelation results presented in Fig. 3, we see that the $\delta_{\mathrm{H\,I}} \times \kappa_{\mathrm{IM}}$ cross-correlation is more powerful; however, the $\delta_g \times \kappa_{\mathrm{IM}}$ correlation we considered here is less prone to systematic effects.

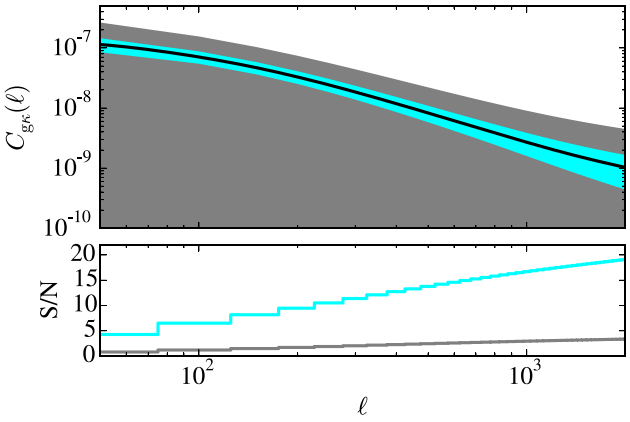

Figure 7. The upper panel shows the $C_{g\kappa}$ cross-correlation power spectrum and measurement errors with LSST and SKA1 (cyan), and LSST and MeerKAT (grey). The lower panel shows the cumulative S/N.

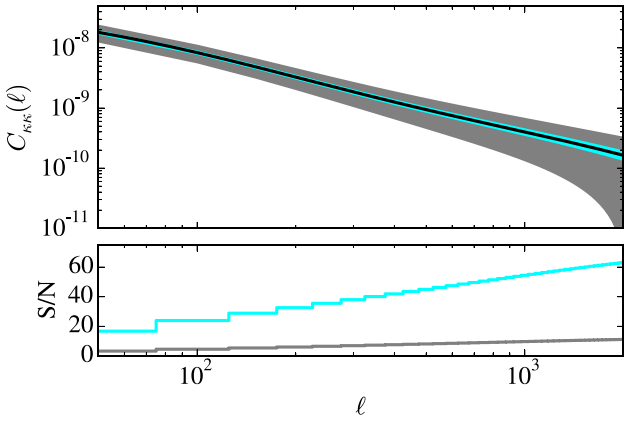

Figure 8. The upper panel shows the $C_{\kappa\kappa}$ cross-correlation power spectrum and measurement errors with LSST and SKA1 (cyan), and LSST and MeerKAT (grey). The lower panel shows the cumulative S/N.

4.4 $\kappa_g \times \kappa_{\rm IM}$ with LSST and MeerKAT/SKA1

Finally, we cross-correlate the lensing convergence κ_g measured with LSST from sources within our chosen bin centred at $z_b = 1$, and $\kappa_{\rm IM}$ measured with the MeerKAT/SKA1 instruments assuming 21 cm sources at $z_s = 1.4$. The results are shown in Fig. 8. We have used $\Delta\ell = 50$.

We see that, in combination with a powerful optical galaxy survey like LSST, both MeerKAT and Phase 1 of the SKA can achieve detection of the lensing convergence coming from 21 cm sources with a high signal to noise. This combination could also alleviate issues arising from systematic effects.

Furthermore, as shown in Pourtsidou & Metcalf (2015), Phase 2 of the SKA (SKA2) can provide high-precision measurements of κ (in auto correlation) at redshifts $z \sim 2$–3. This means that we can use tomographic studies along many redshift bins in order to map the evolution of the growth function at redshifts higher than those of galaxy shear surveys. This will be the subject of future work.

5 DISCUSSION AND CONCLUSIONS

In this paper, we have shown how ongoing and future intensity mapping surveys and optical galaxy surveys can be used to perform high-precision clustering and lensing measurements. We considered a range of H I surveys, concentrating on the performance of the MeerKAT SKA pathfinder, as well as the full SKA Phase 1, and the DES and LSST optical galaxy surveys.

Our auto correlation forecasts show that high signal-to-noise H I detection can be achieved already with the first phase of MeerKAT, MeerKAT-16. This is very important for testing the intensity mapping method and calibrating the H I evolution across redshift using tomographic measurements from MeerKAT and Phase 1 of the SKA.

The measurement of the lensing convergence in auto correlation is much more demanding and heavily depends on the unknown evolution of the H I density (Pourtsidou & Metcalf 2015). Our cross-correlation studies show that using the H I or galaxy density fields in cross-correlation with $\kappa_{\rm IM}$ considerably improves the 21 cm lensing detection prospects. The same is true when using κ_g in cross-correlation with $\kappa_{\rm IM}$. Cross-correlating the galaxy and H I densities will also give us information about the galaxy-H I correlation coefficient. A significant advantage of cross correlating H I intensity mapping and optical galaxy surveys is the alleviation of the issues arising from systematic effects.

The prospects of detecting – for the first time – H I clustering and lensing of 21 cm emission using the intensity mapping technique with the MeerKAT pathfinder are particularly exciting. H I can be detected with high S/N with MeerKAT-16, which is expected to be commissioned in 2016. Using the full MeerKAT instrument in interferometer mode – expected 2017/18 – we have the possibility of detecting 21 cm lensing using IM. This will be an important science achievement of the method and will give us valuable information on how to exploit it for higher redshifts using SKA1.

Clustering and lensing measurements performed using the intensity mapping technique with SKA1 and its pathfinders, as well as cross-correlations with optical galaxy surveys, have a wide range of further cosmological applications. SKA1-MID can measure redshift space distortions across a wide range of redshift ($0 \leq z \leq 2.5$) and is competitive with galaxy surveys like Euclid (Raccanelli et al. 2015). An intensity mapping survey with SKA1-MID can also constrain primordial non-Gaussianity with $\sigma_{f_{\rm NL}} = 2.3$, which is much better than current *Planck* constraints (Santos et al. 2015). In Bull (2016), it was shown that SKA1 IM surveys can yield sub-1 per cent measurements of the linear growth rate, $f\sigma_8$, for $z \leq 1$. The possibility of testing General Relativity at large scales using H I intensity mapping and optical surveys (in combination with CMB lensing surveys) and the $E_{\rm G}$ statistic was investigated in Pourtsidou (2015), showing that sub-1 per cent $E_{\rm G}$ measurements can be achieved. IM observations can be also used to constrain neutrino masses (Villaescusa-Navarro, Bull & Viel 2015).

Finally, we note that in future work we plan to extend these studies to include forecasted constraints on the H I density $\Omega_{\rm H\,I}$, the H I bias $b_{\rm H\,I}$, the galaxy-H I correlation coefficient $r_{\rm H\,I-g}$ and other cosmological parameters.

ACKNOWLEDGEMENTS

This work was supported by STFC grant ST/H002774/1. RBM's work is part of the project GLENCO, funded under the Seventh Framework Programme, Ideas, Grant Agreement n. 259349. The authors would like to thank Philip Bull, Stefano Camera, Roy Maartens and Mario Santos for useful discussions and feedback.

REFERENCES

Abate A. et al., 2012, preprint (arXiv:1211.0310)
Abell P. A. et al., 2009, preprint (arXiv:0912.0201)

Amendola L. et al., 2013, Living Rev. Rel., 16, 6
Ansari R. et al., 2012, A&A, 540, A129
Battye R. A., Davies R. D., Weller J., 2004, MNRAS, 355, 1339
Battye R., Browne I., Dickinson C., Heron G., Maffei B., Pourtsidou A., 2013, MNRAS, 434, 1239
Becker M. R. et al., 2015, preprint (arXiv:1507.05598)
Bigot-Sazy M. A. et al., 2015, MNRAS, 454, 3240
Bull P., 2016, ApJ, 817, 26
Bull P., Ferreira P. G., Patel P., Santos M. G., 2015, ApJ, 803, 21
Camera S., Santos M. G., Ferreira P. G., Ferramacho L., 2013, Phys. Rev. Lett., 111, 171302
Chang T.-C., Pen U.-L., Peterson J. B., McDonald P., 2008, Phys. Rev. Lett., 100, 091303
Chang T.-C., Pen U.-L., Bandura K., Peterson J. B., 2010, Nature, 466, 463
Crighton N. H. M. et al., 2015, MNRAS, 452, 217
Dewdney P., 2013, SKA Project Documents. p. 1
Kaiser N., 1992, ApJ, 388, 272
Kaiser N., 1998, ApJ, 498, 26
Limber D. N., 1954, ApJ, 119, 655
Loeb A., Wyithe S., 2008, Phys. Rev. Lett., 100, 161301
Mao Y., Tegmark M., McQuinn M., Zaldarriaga M., Zahn O., 2008, Phys. Rev. D, 78, 023529
Masui K. W., McDonald P., Pen U.-L., 2010, Phys. Rev. D, 81, 103527
Masui K. et al., 2013, ApJ, 763, L20
Peroux C., McMahon R. G., Storrie-Lombardi L. J., Irwin M. J., 2003, MNRAS, 346, 1103
Peterson J. B. et al., 2009, Astro2010: The Astronomy and Astrophysics Decadal Survey.
Pourtsidou A., 2015, preprint (arXiv:1511.05927)
Pourtsidou A., Metcalf R. B., 2014, MNRAS, 439, L36
Pourtsidou A., Metcalf R. B., 2015, MNRAS, 448, 2
Raccanelli A. et al., 2015, PoS, AASKA14, 031
Rassat A. et al., 2008, preprint (arXiv:0810.0003)
Sánchez-Ramírez R. et al., 2016, MNRAS, 456, 4488
Santos M. G., Bull P., Ferreira P. G., Patel P., Bernardi G., Maartens R., 2014, Technical report. Autocorrelation ECP, available at: https://skaoffice.atlassian.net/wiki/display/EP/ECP+Register+
Santos M. et al., 2015, PoS, AASKA14, 019
Schmidt F., Leauthaud A., Massey R., Rhodes J., George M. R., Koekemoer A. M., Finoguenov A., Tanaka M., 2012, ApJ, 744, L22
Seo H.-J. et al., 2010, ApJ, 721, 164
Smith R. et al., 2003, MNRAS, 341, 1311
Switzer E. et al., 2013, MNRAS, 434, L46
Villaescusa-Navarro F., Bull P., Viel M., 2015, ApJ, 814, 146
White M. J., Carlstrom J., Dragovan M., Holzapfel S. W. L., 1999, ApJ, 514
Wyithe S., 2008, MNRAS., 388, 1889
Zaldarriaga M., Furlanetto S. R., Hernquist L., 2004, ApJ, 608, 622
Zwaan M. A. et al., 2003, AJ, 125, 2842

This paper has been typeset from a TEX/LATEX file prepared by the author.